EUDET-Memo-2007-49

Characterisation and Monte-Carlo study of the T22 Electron Tests Beam Line at DESY II

Hector de la Torre Perez*, Philipp Rahe†

Ingrid-Maria Gregor, Tobias Haas, Ulrich Kötz, ‡

November 30, 2007

Abstract

The availability of test beam lines is essential in the future development of high precision detectors. Therefore the characteristics of the test beam should be well understood.
In this report beam line 22 at the DESY II synchrotron will be characterised. Measurements were performed using the self built detector consisting of a trigger system and a calorimeter. This setup is able to measure rates and energy distributions. To confirm the experimental results, a Monte Carlo simulation of the beam line 22 is done. The results presented in this report were obtained during the summer student program summer 2007.

*DESY summer student 2007, from Universidad Autonoma de Madrid, Spain

†DESY summer student 2007, from Universität Osnabrück, Germany

‡DESY, Hamburg, Germany

1 Introduction

At DESY II there are three test beam lines 21, 22 and 24 available, providing electrons with a specified momentum. These test beams are widely used for research and development mainly of high precision detector components. Therefore the characteristics of the beamlines should be well understood.
During the summerstudent program 2007 we constructed a small detector named *Bacchus*, consisting of a 4-fold trigger system and a lead glass calorimeter. This will be described in section 3.2. Using this setup we measured rates and energy distributions of the test beam line 22, the results are presented in section 4.
These measurements are supported by a Monte Carlo study of the beam line as described in section 5.

2 The Beam Line

As a representative of all three beam lines we performed the following measurements at beam line 22. A bremsstrahlung beam is generated due to the interaction of the electrons in the synchrotron with a carbon target inserted in the beam. The photons generate electron/positron pairs in a secondary target through pair production.

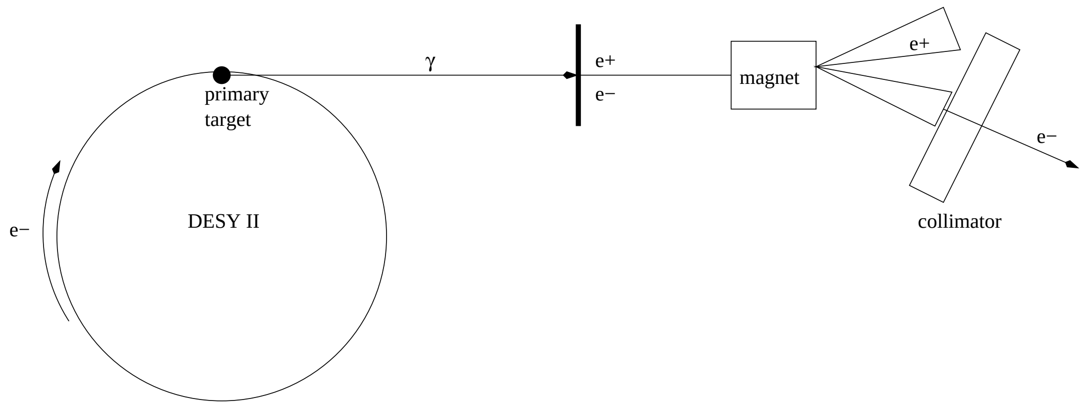

Figure 1: Schema of the Beam line

2.1 Geometry of the Beam Line

According to the plans of the machine group the geometry including the dimensions of the test beam line is shown in Figure 2. This data will be used in the simulation in section 5, we already show some details of the implementation in this Figure: the indicated dimensions and the sensitive detectors.

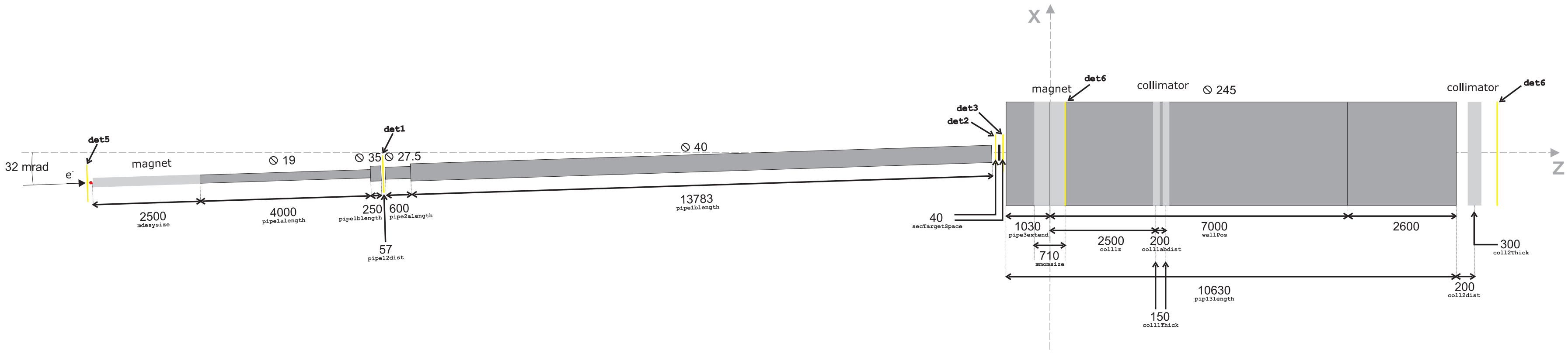

Figure 2: Layout of the beam line

The DESY II electron beam interacts with an inserted fixed target. Two seperately installed primary targets will be examined, one single cylindrical $7\,\mu$m thick carbon fiber and another one consisting of a bundle of carbon fibers, each with a diameter of $7\,\mu$m.
The generated photons are guided through several vacuum tubes, including a crossing of the DESY III ring, to the secondary or converter target.
There are currently 7 secondary targets available in beamline 22. They differ by material and by thickness as listed in Table 1. It has to be taken into account that before the converter targets the vacuum system is sealed off with 0.5 mm thick aluminium windows. The test will show that pair production takes place in this material as well as in the converter targets.

material	thickness	size
Cu	1 mm	$45 \times 60\,\mathrm{mm}^2$
Cu	3 mm	$45 \times 60\,\mathrm{mm}^2$
Cu	5 mm	$45 \times 60\,\mathrm{mm}^2$
Cu	10 mm	$45 \times 60\,\mathrm{mm}^2$
Al	1 mm	$45 \times 60\,\mathrm{mm}^2$
Al	3 mm	$45 \times 60\,\mathrm{mm}^2$
Al	4 mm	$45 \times 60\,\mathrm{mm}^2$

Table 1: Available secondary targets at the beam line 22

After the conversion the electron momentum is selected using a dipole magnet controlled by the user. The current in the magnet is linear to the selected momentum, for details see section 2.3. The final beam is formed using two collimators, one which is controllable on the spot from the control room and located after the magnet and another one, which has a fixed size of $12 \times 12\,\mathrm{mm}^2$, is located in the experimental area. A study of the characteristics of the collimators and their influence on the beam is included in section 4.1. For consistency we name the opening of the collimators by a tuple $(a, b; c, d)$ where a and b denote the vertical and c, d denote the horizontal opening measured from the middle in both directions, cp. Figure 3.

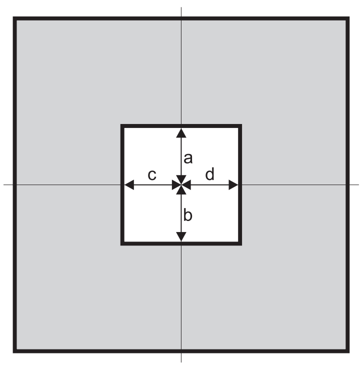

Figure 3: Sizes of collimators

2.2 Physics of the Beam Line

The usual parameters of the DESY II beam during this experiment were an momentum of 6.97 GeV and a current of 1.8 ± 0.2 mA, which is equivalent to $\approx 1 \times 10^{10}$ e/bunch.
Bremsstrahlung is created by interaction of the circulating electrons with the inserted fiber. As the critical energy for carbon is $E_c \approx 84$ MeV [3] the particles in the considered regime are minimal ionising particles (MIPs). The spectrum of the generated photons has a $1/E_\gamma$ dependence with a cut at the energy of the primary electron beam.
After approximately 20 m guidance in vacuum pipes the photons are converted to electron/positron pairs by pairproduction in the secondary targets. The production takes also place in the 0.5 mm thick aluminum window at the end of the vacuum pipe through DESY III ring. The total cross section of pairproduction in the regime of $1 \ldots 6$ GeV is nearly flat.
In contrast to this simple physics explanation, the actual behaviour of the beam is full of side effects and affected by many processes along the path from the primary target to the experimental hall. Therefore we will provide enough experimental data in order to characterise precisely the real behaviour of the beamline. The experimental results will be supported by a Monte Carlo simulation in section 5.

2.3 The Momentum Selection

The dipole magnet at the beamline 22 is of type MR with an integrated magnetic length of 710 mm, it can be operated up to a maximum current of 375 A. The linear relation between the current and the momentum was given by the machine group. We measured with a 1 mm Cu target the energy response of the calorimeter against the selected current, proportional to the desired momentum. The result is shown in Figure 4 and verifies the dependence between measured energy and current in the magnet within the normal operation range. A linear fit reveals a linear term and a ADC pedestal:

$$E_{ADC} = (174 \pm 4) \cdot p \text{ [GeV]} + (66 \pm 13)$$

During this measurement the collimator setting was $(5.0, 5.0; 1.0, 1.1)$.

3 Experimental Description

3.1 The Detector Setup

All parts of the detector were made light tight, tested and mounted onto an aluminium platform. Two aluminium support frames for each pair of trigger scintillators was tightened down to the platform. The whole setup was aligned to the beam line axis using motorized supports operated from the control room. The best alignment was reached searching for the maximum rates in both axis.

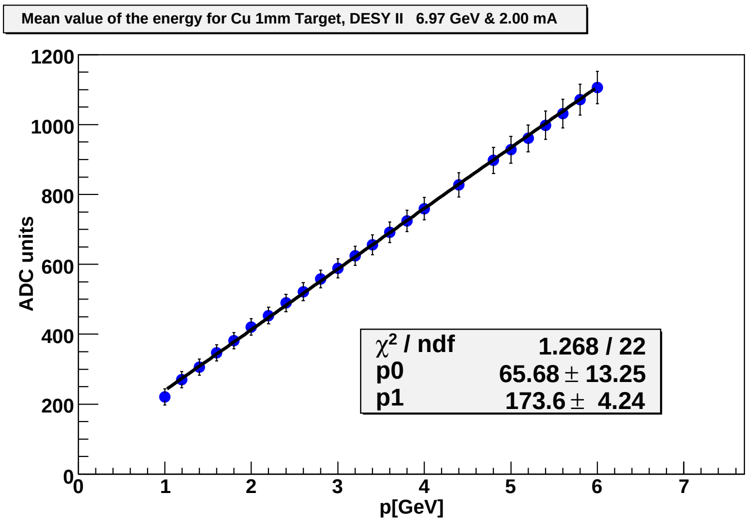

Figure 4: Mean energy recorded with the calorimeter against current and momentum

3.2 Description of the Detector

3.2.1 The Trigger System

The trigger system was build using four scintillator counters, made of $30 \times 9\,\mathrm{mm}^2$ pieces scintillating material of 2 mm thickness. Each scintillator is connected to a Hamamatsu H5783 PhotoMultiPlier (PMT) with a built-in Cockroft Walton type base. These photomultipliers therefore do not need an external high voltage supply. The four scintillators are separated in two pairs and fixed as shown in Figure 6 with a distance of 400 mm between them. This setup is able to select a beam area of $9 \times 9\,\mathrm{mm}^2$. The coincidence rate of this 4-fold trigger system has been measured as the rate of the electron beam during the experiment.

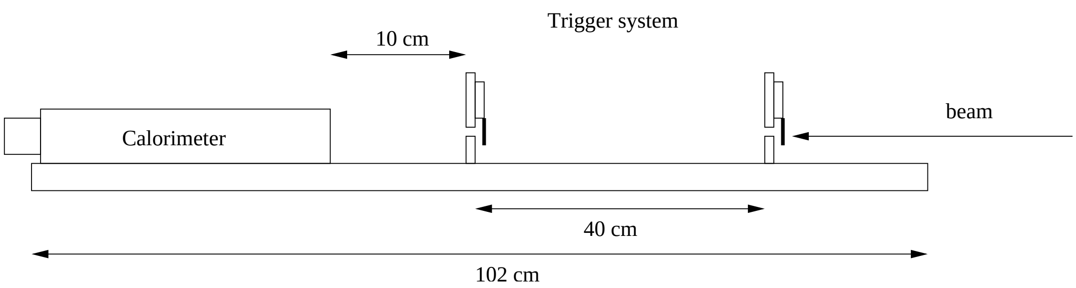

Figure 5: Schema of the detector

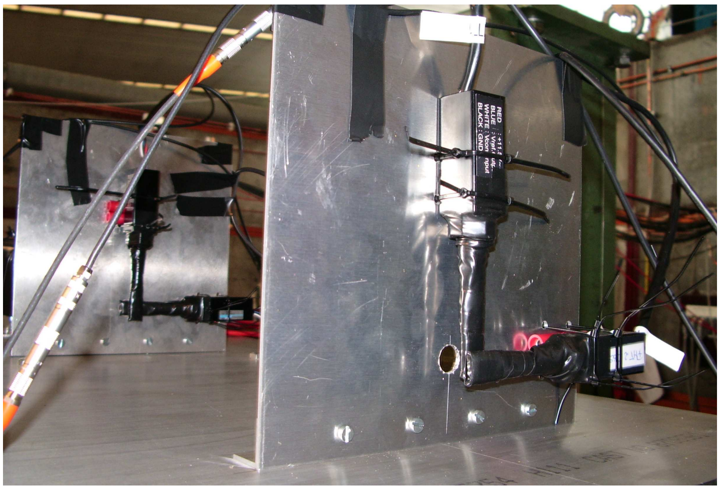

Figure 6: Photo of the trigger system

To study the divergence of the beam and the different efficiencies of the four triggers, we measured the rates using only each pair of triggers separately. With this method also particles are accounted for which are not traveling in straight tracks. This increase in the particle rate, compared to the normal rate using the 4-fold trigger, is ssummarised in Table 2. With a max increase of 50% compared to the 4-fold configuration, one can conclude that the beam is not parallel but divergent. With a 4-fold coincidence and a long enough distance (30 cm) between the front and the back trigger scintillator pair the triggered electrons are likely to be parallel to the beam axis.

Momentum	Only back pair	Only front pair
1.0 GeV/c	50 ± 10 %	50 ± 10 %
2.0 GeV/c	42 ± 3 %	44 ± 3 %
3.0 GeV/c	32 ± 2 %	48 ± 3 %
4.0 GeV/c	21 ± 2 %	42 ± 3 %
5.0 GeV/c	30 ± 4 %	51 ± 6 %
6.0 GeV/c	30 ± 10 %	40 ± 10 %

Table 2: Increase of particles detected using only one pair of triggers in comparison with the normal 4-fold configuration

3.2.2 The Lead Glass Calorimeter

The calorimeter as shown in Figure 7 is made of one $10.7 \times 8.5\,\text{cm}^2$ cross section and 33.3 cm thick (equivalent to 14.8 radiation lengths) lead glass block, previously part of the calorimeter of the Jade detector. It is connected to a PMT Hamamatsu R594 by a 6 cm light conductor (OHARA BK7) [5], which needs a 1.2 kV source to work. For 6 GeV/c electrons the shower length in lead glass is $\approx 5.4 \cdot X_0$ so the electrons of the beam are going to loose all their energy within the calorimeter block. We also have some Čerenkov radiation produced into the lead glass, due to the high velocity of the incoming electrons and the high refractive index of the lead glass, but it won't affect the measurements because the energy and number of the Čerenkov photons is completely flat in our regime 1...6 GeV/c [3]. The photons produced in the shower will be registered in the PMT and read out using a 16 bit, 8 channel, charge integrating ADC (Analog to Digital Converter). This method provides an easy way to measure the shape of the energy distribution of the electron beam and to compare the energy for different momentum selection. In contrast, without a precise calibration it is not possible to give an absolute value for the energy. It is also important to notice for upcoming use of the calorimeter that the energy measurement is not independent of the HV, both in absolute value and for comparison porpouses. The behaviour of the calorimeter for different HV was studied and included in the appendix, Figure 31.

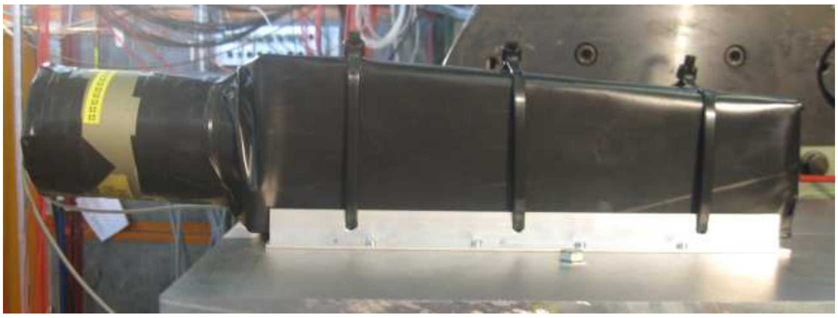

Figure 7: Photo of the calorimeter

3.2.3 The Electronics

The trigger system is set up by connecting the four scintillators to a fast discriminator and then to a 4-fold coincidence module. This trigger signal is used as a gate for the ADC. Whenever the four scintillators receives a hit signal within the coincidence time a gate is generated and the ADC accepts the signal coming from the calorimeter, registering data proportional to the electron energy. Figure 8 shows a diagram with the different connections. The appearance of the gate signal, coming directly from the coincidence module and the calorimeter signal are shown in Figure 9. The signal from the calorimeter was delayed in order to compensate different cable lengths, and the signal from the coincidence modul was elongated to detect the full calorimeter data within the gate time.

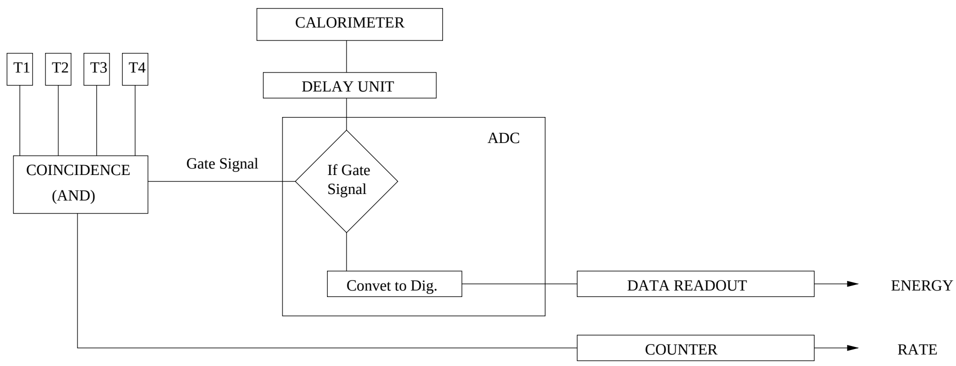

Figure 8: Schema of the logical connections

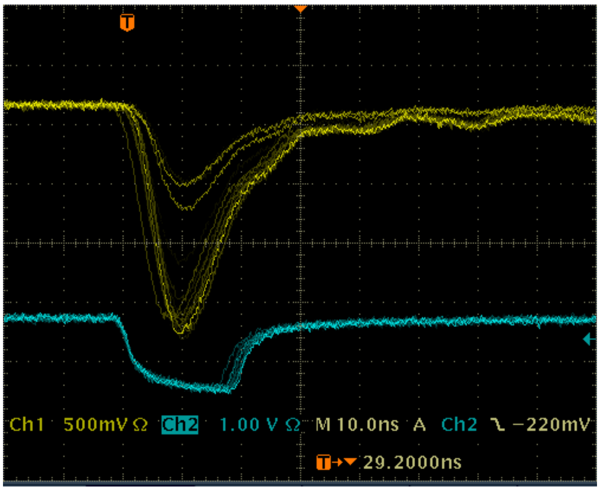

Figure 9: Signal of the Calorimeter (top) and the unelongated signal from the coincidence (bottom)

3.3 Methods for data analysis

The data from the ADC was read out using a modified version of the software designed and provided [4]. The program reads all eight ADC channels and stores this data into a ROOT histogram. The ADC is collecting data within the gate time and generates a number integral to the amount of charge stored in this time. The program reads this number and fills the appropiate bin. The charge stored during the gate time is proportional to the signal produced in the calorimeter and thus proportional to the momentum of the electrons. Therefore the x-axis of the histogram is proportional to the energy and the height of each bin represents the number of hits in the calorimeter for each “energy”. One of these histograms is shown as an example in Figure 10 and consist in two peaks, one large one and one small peak in higher values of the x-axis. The analysis of these histograms is made by a ROOT script with the following steps:

- The histogram is read out from the ROOT file.

- It is cleaned from background using the ROOT object `TSpectrum` and his class `Background`, smoothing the lines and making easier to fit and identify the different peaks. The typical output of this process is shown in Figure 10.
- The maximum of the new histogram is identified and a gaussian fit is applied. The parameters of this fit are used to analyse the width and mean value of the primary peak, corresponding to the main energy of the electrons hitting the calorimeter.
- To clearly identify the secondary peak, the first peak is removed from the plot by introducing a lower limit of 1100 ADCs. Once the secondary peak is isolated the proccess is repeated and the new values of the gaussian fit are used to analyse it.
- The number of hits under the primary and secondary peak are determined using the above mentioned fits to constrain each peak region. These are compared with the total number of hits to obtain the approximate ratio of electrons that are part of each peak and have a numerical estimation of the secondary peak.

Once each value of the energy, width and number of hits of both primary and secondary peaks are obtained, they are stored in an `TNtuple` for later use and analysis. All the results are included in section 4

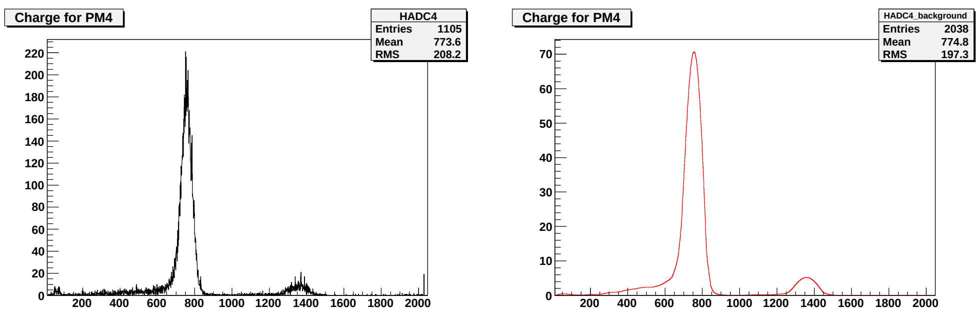

(a) One histogram just read out from the ADC

(b) The same histogram after being cleaned

Figure 10: ADC readout and signal processing

4 Experiment

It is crucial to mention that, during each run of measurements, the beam in DESY II is not perfectly stable, and that this oscillations can affect the results. As a reference, the behaviour of the beam during the measurement's time is included in Figure 11. The meassurements took place from 17:10 on.

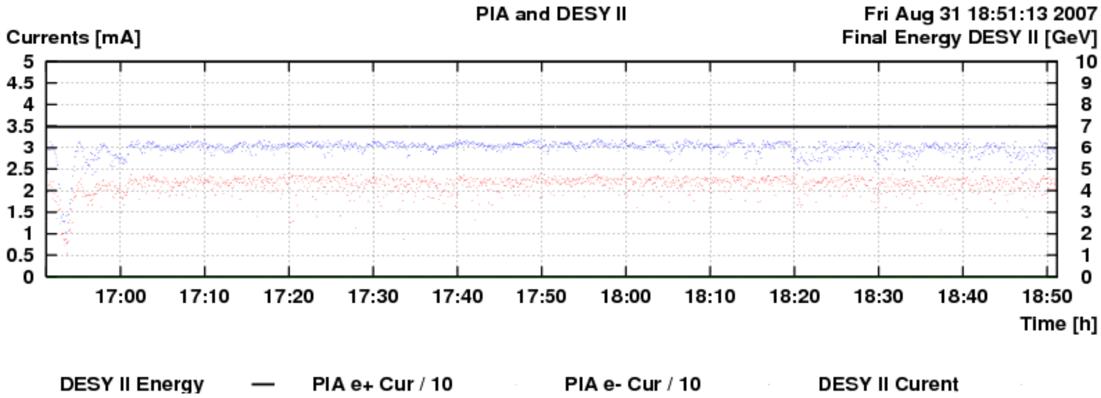

Figure 11: Energy (top) and current (bottom) of the beam during the measurements

4.1 Influence of the Collimators

To check the beam profile and the energy distribution rates and ADC counts at different sizes of the collimator were measured. The results are shown in Figure 12. The method for analysing the data is described in section 3.3.

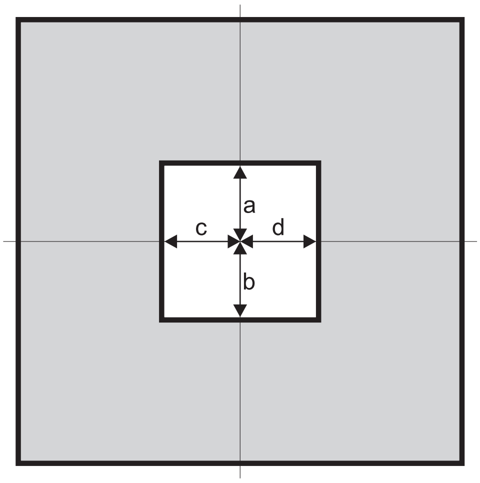

(a) Rates against different collimator aperture

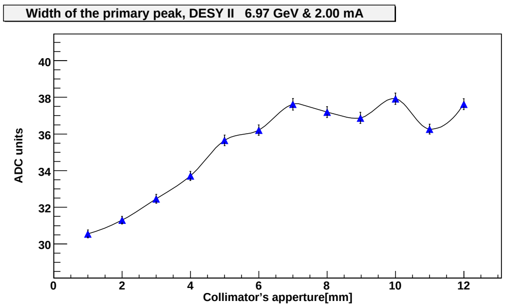

(b) Energy width against different collimator aperture

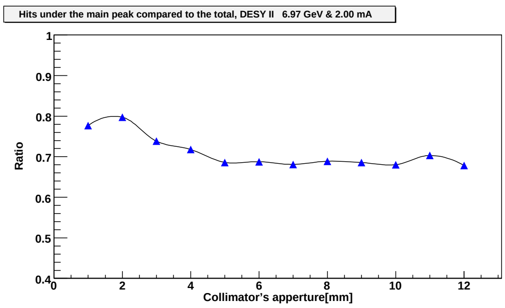

(c) Ratio between hits under the primary peak and total hits

Figure 12: Different profiles of the primary collimator. Please not the offsets in the y-axis for figure (b) and (c).

Due to deflections only occuring horizontally the rates are larger in horizontally direction than in vertical direction. As expected and shown in Fig. 13 the mean of the energy is constant.

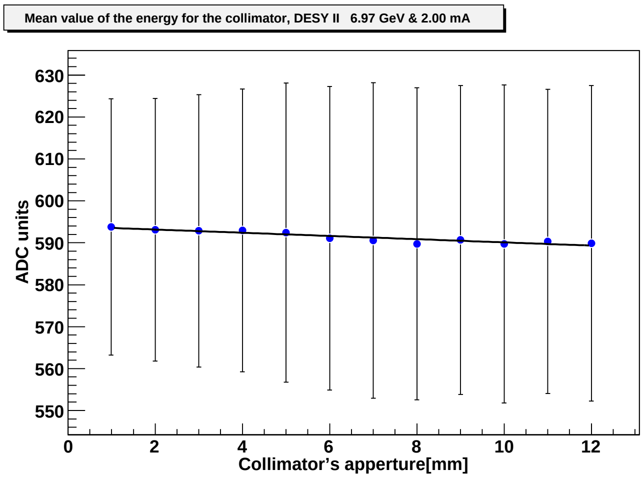

Figure 13: Mean value of the primary energy peak for different collimator sizes.

The width remains constant from approximately an opening size of $10 \times 10\,\mathrm{mm}^2$. The active size of the 4-fold trigger system is $9 \times 9\,\mathrm{mm}^2$ and the second collimator has an opening of $12 \times 12\,\mathrm{mm}^2$. The beam contamination regarding the energy distribution remains constant from about $(5.0, 5.0; 5.0, 5.0)$.

4.2 Rates for Different Converter Targets

The rates for the different converter targets which are listed in Table 1 were measured in in 1.0 GeV steps, while DESY II was operating at 6.97 GeV with an indicated current of $2.1 \pm 0.2\,\mathrm{mA}$. The collimator was opened to $(5.0, 5.0; 5.0, 5.0)$. The results of this measurement are shown in Figure 14. For thicker targets higher rates were observed, but the rates do not increase linearly with the thickness of the target. Secondary processes, such as multiple scattering and start of showering, suppress the linearity.

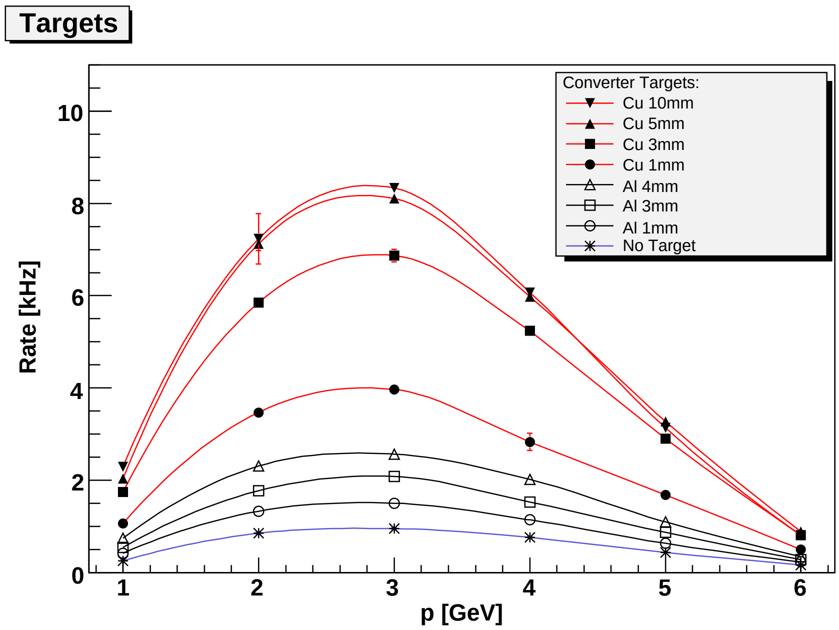

Figure 14: Rates for different converter targets against selected momentum

Furthermore one would expect higher rates at lower energies. In Figure 14 shows a maximum around 3 GeV. Reasons are a larger divergence and mor multiple scattering for lower momentum particles. In order to understand all effects involved a Monte-Carlo simulation was set up.

4.3 Energy Measurements

The energy detected in the calorimeter for each selected momentum, from 1 GeV to 6 GeV was measured. As described in section 3.3 this is achieved by analysing the primary peak of the distribution. The energy for all targets is shown in Figure 15 and, as expected, has no dependence at all on the different materials and increase linearly with the selected momentum. The width of the primary peak is shown in Figure 16 and shows that the primary peak is broader for higher momentum and thicker targets thus implying broader energy distribution for the electron beam around the mean value. The treatment and conclusions for this dependence needs the simulation data and therefore is included in section 6.

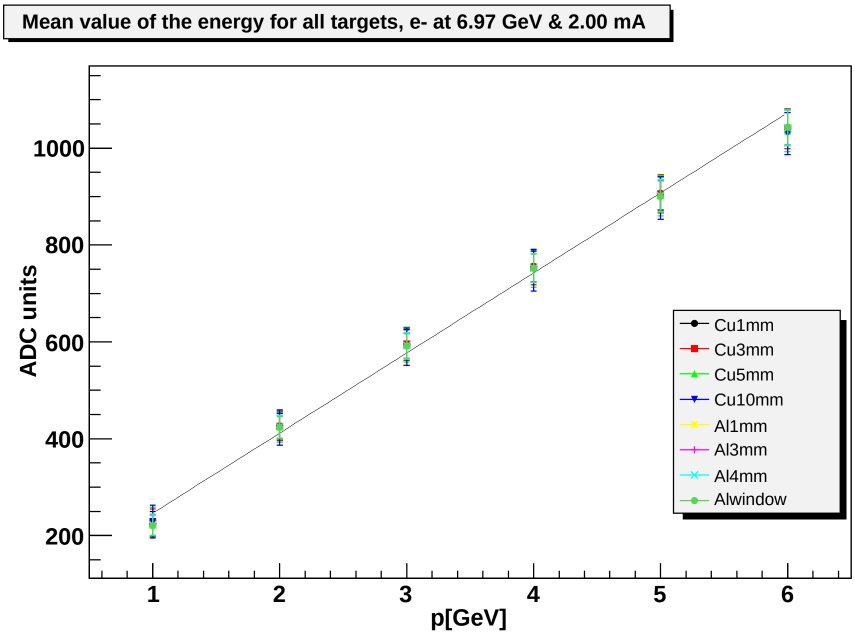

Figure 15: Energy mean for different converter targets against selected momentum

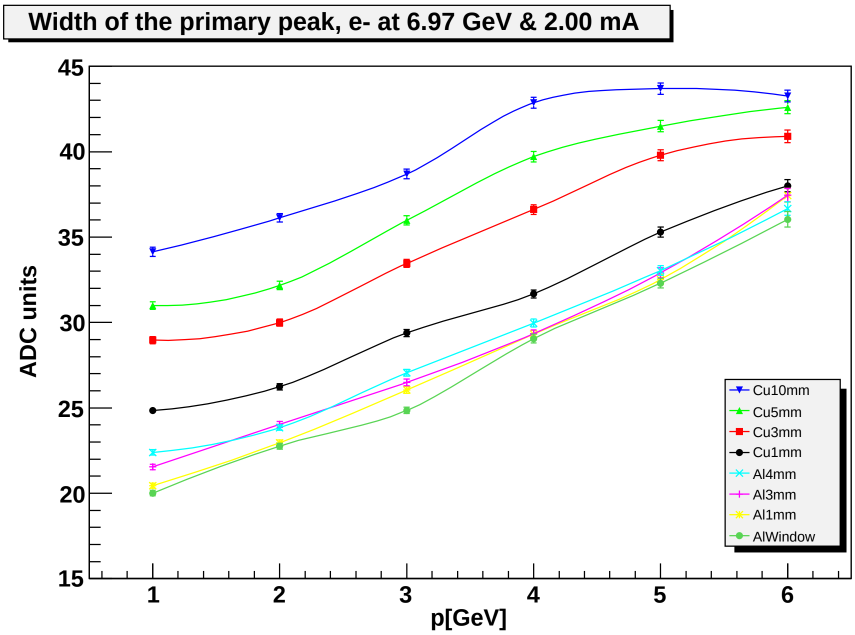

Figure 16: Width of the primary peak for different converter targets against selected momentum

4.4 Secondary Peaks in the Energy Distribution

As explained in section 3.3, a secondary peak at higher ADC values is visible in nearly all histograms. In Figure 17 it is shown that the mean value of this peak increases linearly with the selected momentum and it is approximately two times the mean value of the main peak, not showing any dependence on the converter target material. The width is shown in Figure 18. It is assumed that this peak represents a second electron hitting the calorimeter within the gating time. Therefore a signal with double energy is registered.

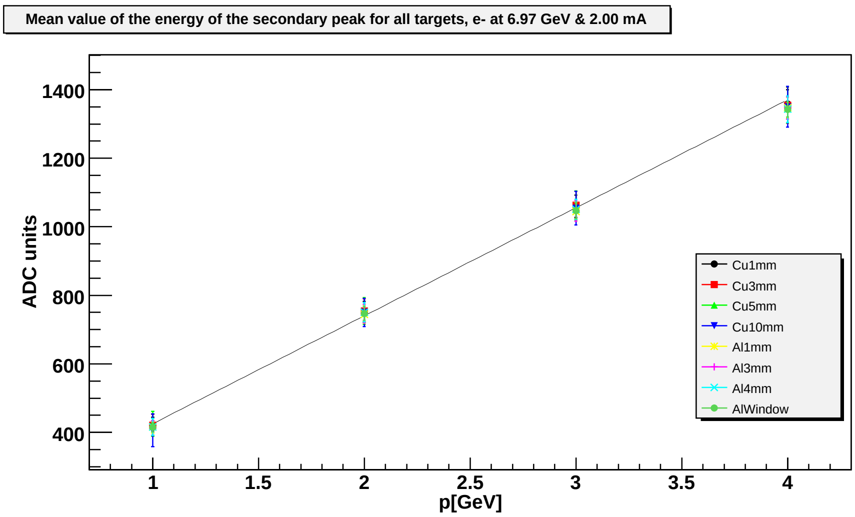

Figure 17: Mean energy of the secondary peak for different converter targets agains selected momentum

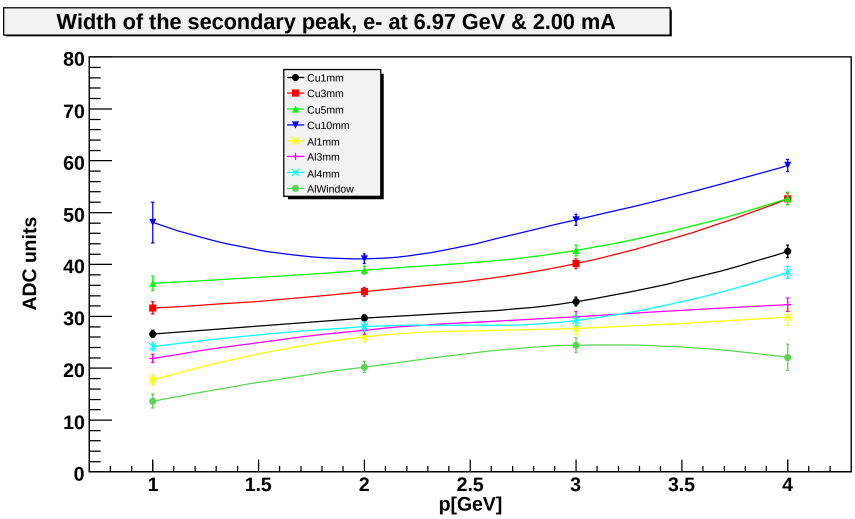

Figure 18: Width of the secondary peak for different converter targets against selected momentum

The ratio of how often this proccess happens compared to the total number of hits is shown in Figure 19 and it does not change significantly with the selected momentum, being much more sensitive to the material and thickness of the converter target. It is shown that with a thin target of a low Z material the beam is much cleaner an suppresses secondary hits.

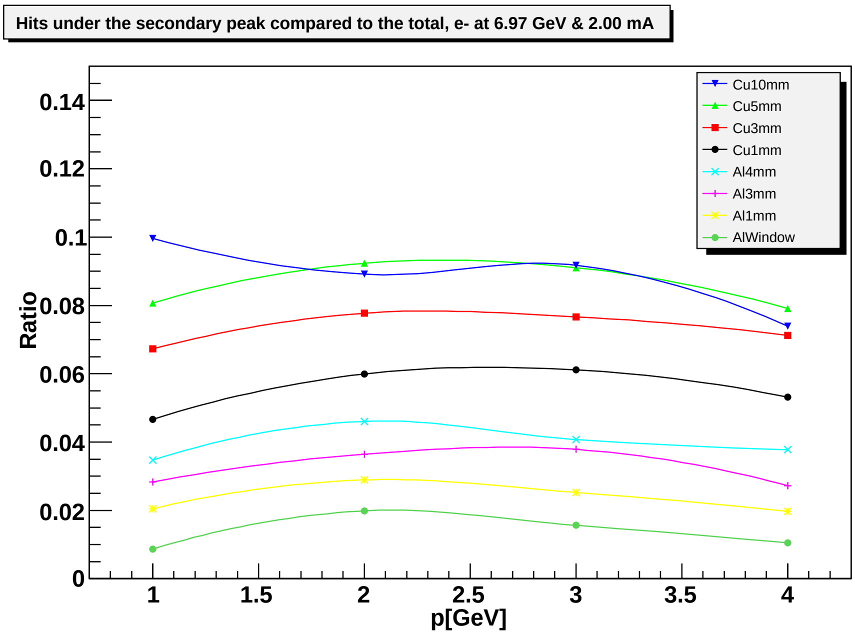

Figure 19: Ratio of the hits under the secondary peak compared to the total for different converter targets against selected momentum

4.5 Testing the Fiber Bundle

One of the consequences of the upcoming construction of PETRA III at the DESY site is, in order to fullfill the requirements of this syncrotron source, that DESY II will be required to run with positrons. This running mode would imply lower current of primary particles and therefore lower rates in the test beam [1]. One of the ideas to obtain higher rates with low current is exchanging the single primary target by a bundle of carbon fibers. The rates were measured while DESY II was running 3 GeV/c ($\approx$ 1.3 $\times$ 10^9 electrons/bunch), using a Cu 1 mm converter target and the mentioned fiber bundle. For safety reasons a very low current in DESYII was selected resulting in a less stable current. The rates of the single fibre were measured at a starting current value of 0.27 mA, but this dropped to 0.13 mA during the measurement. With the single fibre a rate of 770$\pm$20 Hz was measured. When inserting the fibre bundle this rate increased to 2500$\pm$100 Hz. Taking the current drop in the machine into account a gain of a factor of six from the usual target setup was observed.
The beam behaviour during the insertion of the new target was also monitored. Figure 20 shows the influence on the beam when inserting the fibre bundle target. Further studies will be made concerning the beam behaviour. In addition the simulation of multiple-fiber targets will be studied and is included in section 5.

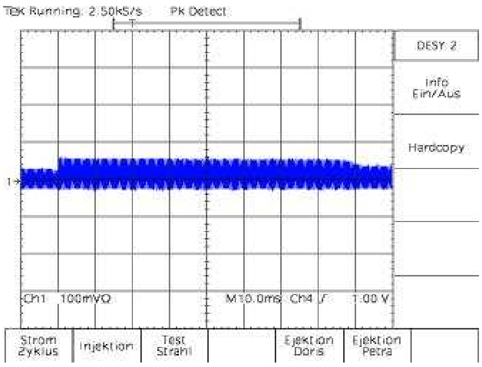

(a) Without carbon fiber

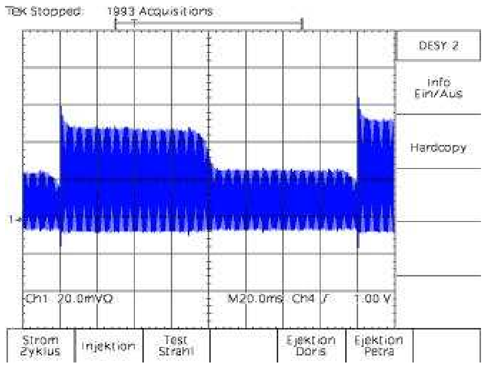

(b) Single carbon fiber

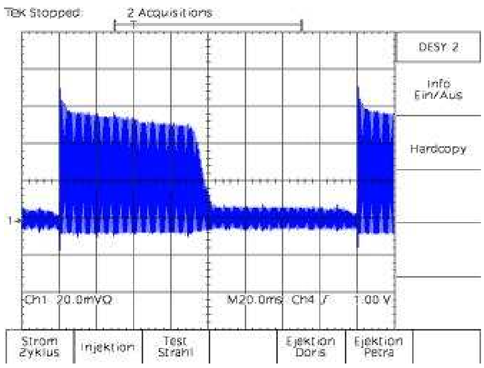

(c) Fibre bundle

Figure 20: Beam intensities of DESY II

5 Simulation

In order to analyse the characteristics of the beam line 22 we support the measurements by a Monte Carlo simulation using GEANT4. The crucial part was defining the geometry. We ran the program on two standard PCs, doing a few hundred runs each consisting of 10000 primary electrons took about 8 hours. Simulating a whole bunch containing about 10^9 electrons was not possible on these machines, but there will be future applications on the grid.

5.1 Class layout

The program is splitted in several classes which will be shortly described. The main program `exampleN02.cc` initialises all classes required to run the simulation:

- `ExN02DetectorConstruction` defines the geometry of the beam line as well as the magnetic fields and the sensitive detectors.

- `ExN02PrimaryGeneratorAction` constructs the primary electron beam of DESY II. It uses coordinates defined in `ExN02DetectorConstruction`.
- `ExN02PhysicsList` specifies the used physical processes and involved particles.
- `ProfileSD, PipeGammasSD, BfrColElecSD, AftrColElecSD, MomMagSD` and `EndPipeSD` are the sensitive detectors used to obtain data.

5.2 Defining the Geometry

We simulate all parts of the beam line 22 that are important for the beam characteristics. The origin of the used coordinate system is the middle of the momentum selecting magnet. The angle between the upstream and the downstream part seen from this magnet is 32 mrad, so the upstream part of the beamline is rotated. The downstream part is aligned along the z-axis.

- Vacuum pipes: According to the drawings from the machine group we define iron pipes with different diameters and a wall thickness of 1.5 mm. The 0.5 mm thick aluminium and 0.2 mm thick kapton windows are defined as well.
- Carbon fiber: The fiber has a diameter of 7 μm. The probability for interaction with the beam is very low so it is essential to use a high number of events. The fiber bundle is modelled as well. As the lateral extension of the modeled beam is smaller than the diameter of the fiber, the bundle is simulated as `fiberNumber` fibers orientated along the beamline.[1]
- DESY II electrons: We define the DESY II beam as normally distributed electrons with $\sigma_x = 350\,\mathrm{nm}$, $\sigma_y = 35\,\mathrm{nm}$[2], generated a few microns straight in front of the fiber. In order to separate primary electrons from created photons we define a magnetic field right behind the fiber guiding the electrons away from the setup. As the field strength is large there are sometimes problems with the particle tracking in the program. These problems do not effect the produced gammas so it is acceptable to ignore the warnings.
- Secondary target: We simulate the targets used in the experiment as listed in Table 1. In order to get high rates we will use mainly the Cu 10 mm target.
- Momentum selecting magnet: A section of the vacuum pipe behind the secondary target contains a magnetic field oriented in y-direction to separate the momentum of the electron/positron pairs.
- Collimators: Parts of the inside of the vacuum in the pipes are defined as lead, containing slits of specified size[3].

[1] This has to be done different in future simulations as the beam has actually a dimension of 1 mm
[2] real size: $\sigma_x = 1\,\mathrm{mm}$, $\sigma_y = 0.5\,\mathrm{mm}$
[3] material needs to be checked

- A concrete wall is defined to keep the experimental area free of scattered particles. One can easily define future applications in this part of the beamline.

The rendered geometry is shown in Figure 21. For further details about the used dimensions see Figure 2.

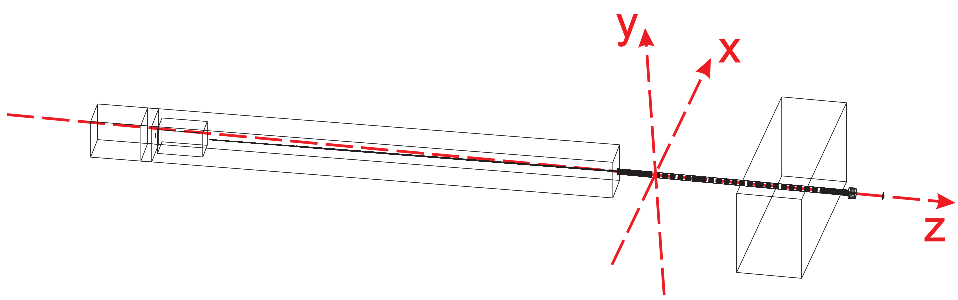

Figure 21: Rendered geometry of the simulated test beam line 22

5.3 Physical Processes taken into Account

In GEANT4 it is necessary to define the physical processes (as i.e. electromagnetic, hadronic, ...) for which the cross sections are calculated as well as which particle should be used. To simplify the calculation we used the following electromagnetic processes:

- bremsstrahlung
- photoelectric effect
- compton scattering
- multiple scattering
- gamma conversion
- ionisation

which are attached to the following particles:

- γ
- e^+, e^-, μ^+, μ^-
- π^+, π^-, K^+, K^-

5.4 Data Acquisition

To get the output of the data the concept of *sensitive detectors* is used. With a sensitive detector attached to a volume it is possible to register every particle tracking through this volume. Filters for particle types, energy and momentum are applied and spatial resolution is achieved. We use 6 detectors of this kind:

- To control the profile of the primary beam (`ProfileSD`, `det5`).
- To get information about the bremsstrahlung in between vacuum pipes 1 and 2 (`PipeWindowSD`, `det1`)
- and before the the secondary target (`BfrColSD`, `det2`).
- To have a look at the converted electron/positron pairs (`AftrColSD`, `det3`).
- To control the momentum selecting magnet (`MomMagSD`, `det6`).
- Finally to get the profile of the beam in the experimental area (`EndPipeSD`, `det4`)

Each hit is stored in a `NTuple` saved in a ROOT file and analysed with the current ROOT version 5.14.00. We coded a root script `analyseSim.c` creating histograms and saving them as `png` or `eps` files. A well arranged LaTeX document can be created using the `analyseSim.tex` template.

5.5 Results

The simulation is giving us information about the beam line concerning the beam profile and the influence of different secondary targets, fiber bundles as primary targets and different distributions of the primary electrons. Due to time reasons not all secondary targets could be simulated, only Al 5 mm, Cu 5 mm and Cu 10 mm were included in the simulation.

5.5.1 Beam Profile

Using the sensitive detectors we are able to measure the spatial extend of the beam. We obtained the following plots using a single fiber with a diameter of $7\,\mu$m and a secondary target of Cu 10 mm. We used 1200×10000 primary electrons with a momentum of 7.0 GeV. In the detector in the experimental area we want electrons with a momentum of about 3 GeV, therefore the magnetic field in the momentum selecting magnet was chosen to be $-0.5\,$T.

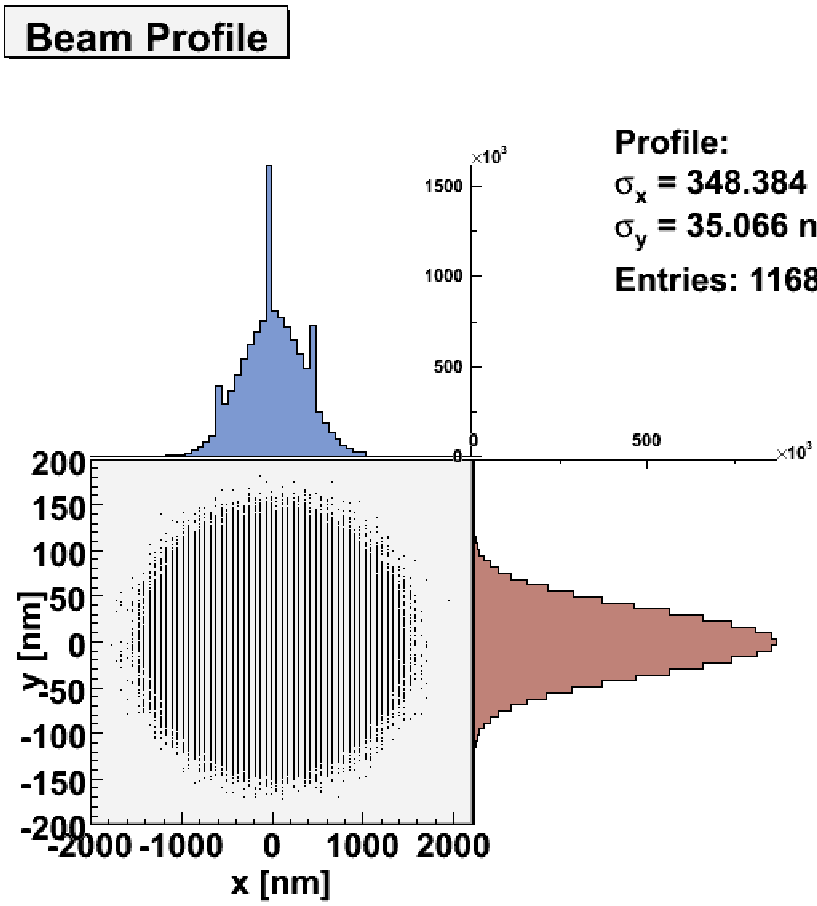

Figure 22: Profile of the primary beam.

The primary beam profile as shown in Figure 22 reflects the used parameters σ_x and σ_y. We assume that discretization along the x-axis resulting in the plotted lines is an effect of the random number generator.

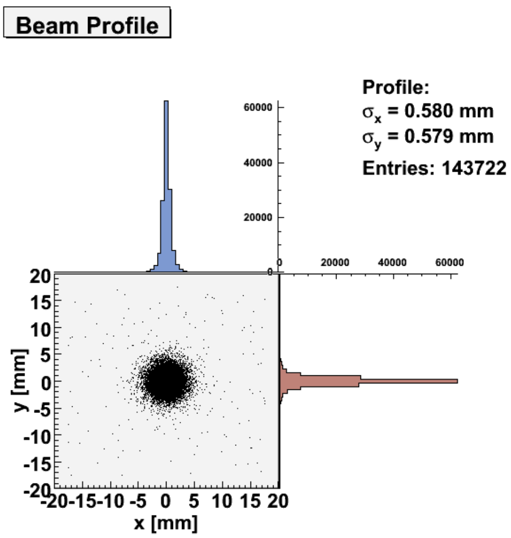

(a) Gammas in the pipe window, 6.8 m behind the carbon fiber

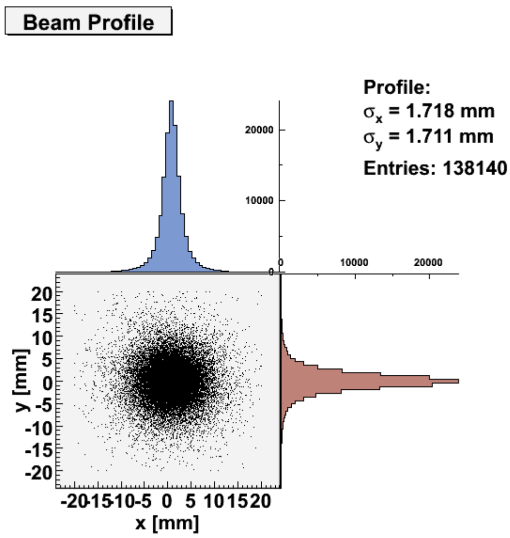

(b) Gammas in front of the converter target, 21.2 m behind the fiber

Figure 23: Profile of the converted gammas.

Taking the data of Figure 23 into account the gamma beam has an opening angle ϕ of

$$\phi \approx 0.16\,\text{mrad}.$$

After the pair production the distribution width of e^+ and e^- increases, as shown in Figure 24.

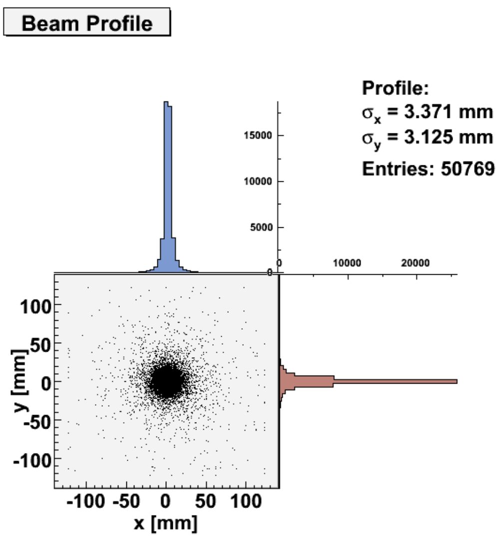

Figure 24: Profile of the converted e^+/e^- pairs.

As expected the beam widens behind the momentum selecting magnet, cf. Figure 25.

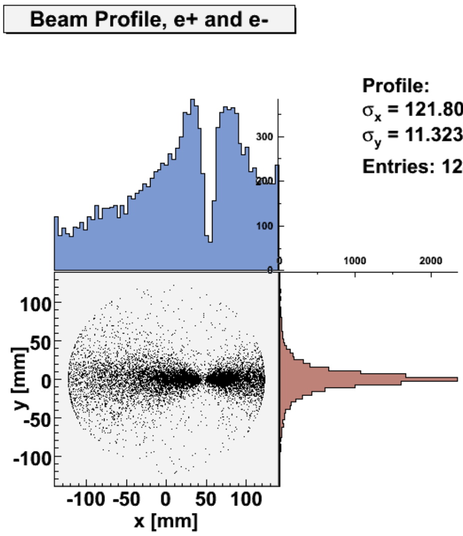

(a) Profile of the e+/e- beam

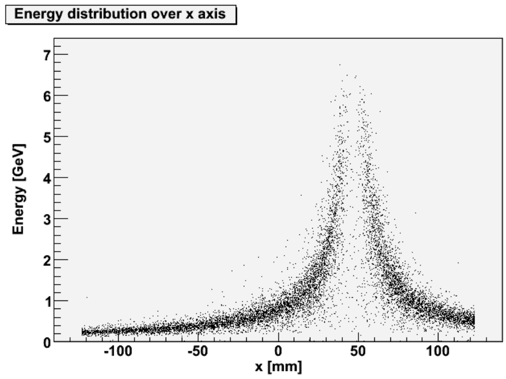

(b) Distribution of the energy along the x axis

Figure 25: Profile behind the momentum selecting magnet.

In Figure 26 the small rates in the experimental area are shown.

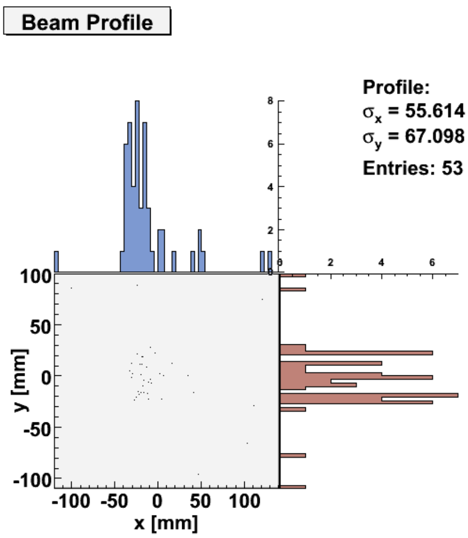

(a) Profile

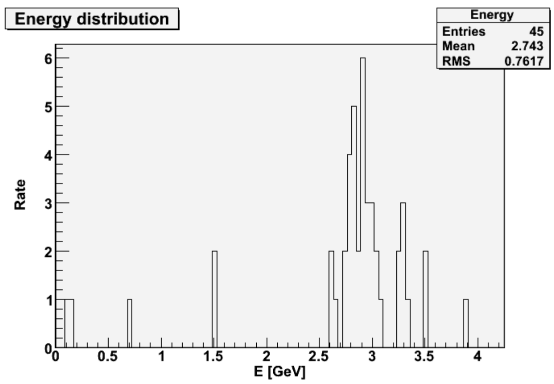

(b) Distribution of the energy

Figure 26: Electron beam in the experimental area

5.5.2 Energy Distribution

It is helpful to have a look at the energy distribution of the gammas generated in the carbon fiber and of the e^+/e^- pairs generated in the secondary target. The primary electrons have a momentum of 7.0 GeV.

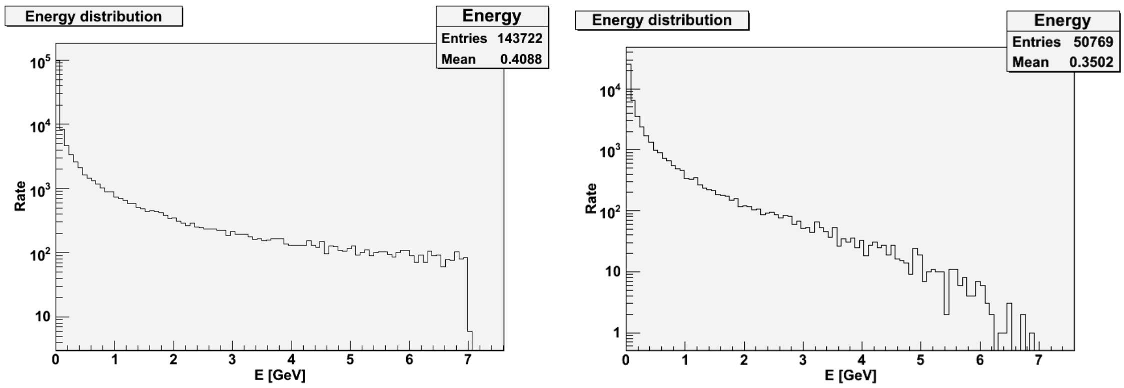

(a) Gammas (b) e^+/e^- pairs

Figure 27: Energy distribution of generated gammas in the carbon fiber and of generated e^+/e^- pairs in the secondary target.

The $1/E$ dependence of the gammas can easily be seen and with higher momentum particles are lost.

5.5.3 Concerning the Momentum Selection

Although we didn't have numerous events in the end pipe detector we try to figure out the dependence between the magnetic field and the selected momentum. As fitting of gaussians to the little number of events is difficult we just take the mean and root mean square at the given energies, resulting in large error bars. The energies at the zero point in the histograms are neglected, their origin are tracking problems. The result is shown in Figure 28, we have a linear dependence as from the experimental result.

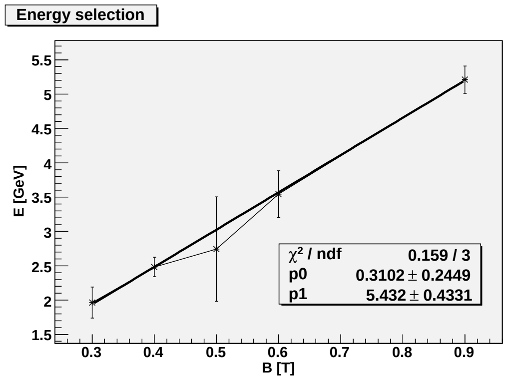

Figure 28: Mean of selected momentum in comparison to the applied magnetic field strength.

5.5.4 Fiberbundle

As mentioned before one idea to increase the rates during the parallel running of DESY II and PETRA III is to use a bundle of fibers. We implement a bundle of 5 fibers into the simulation, the fibers are aligned along the beam axis. Comparing the rates after the secondary target for a single fiber and a fiber bundle we gain a factor of 1.3 in the number of hits compared to a single fiber.

5.5.5 Angular Distribution of the Primary Particle Momentum

The momentum of the electrons in the DESY II is assumed to have an opening angle of 0.5 mrad. We therefore apply a Gaussian distribution with $\sigma_\phi = 0.5\,\mathrm{mrad}$ to the primary particle momentum and compare the beam profiles in front and behind the secondary target as shown in Figure 29.

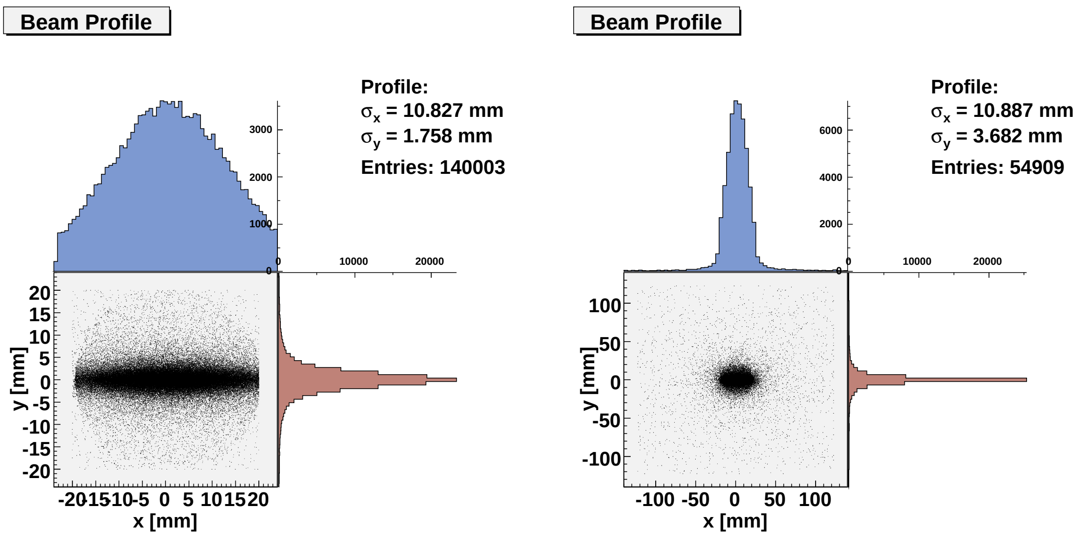

(a) Profile of the gamma beam in front of the secondary target

(b) Profile of the e^+/e^- beam behind the secondary target

Figure 29: Profile using an angular distribution of the primary electron momentum.

The beam size along the x-axis increases for about a factor of 6.3, the opening angle of the gamma beam is $\phi = 0.5\,\mathrm{mrad}$. As seen in Figure 30 the distribution of hits in the experimental hall detector remain similar, but the rate decreases by a factor of 0.4.

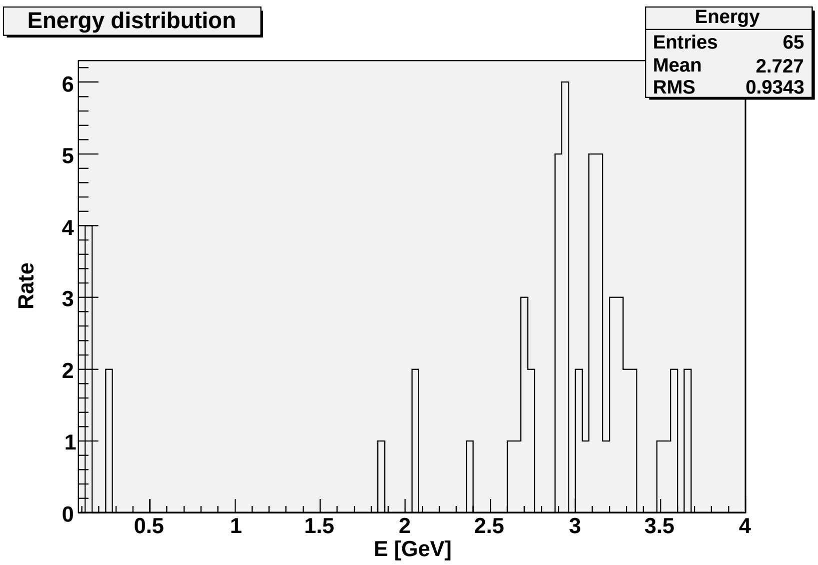

Figure 30: Energy distribution in the experimental hall detector.

6 Comparison of Experiment and Simulation

For a comparison of the measured rates and energy distribution with the simulated data the number of runs have to be some order of magnitude higher, we were not able to run this on our computers. Nevertheless we are able to give some explanations.
In Figure 16 we discovered an increasing width of the primary energy peak with higher selected particle momentum, we compare these results with the momentum distribution along the x-axis at the sensitive detector behind the momentum selecting magnet as shown in Figure 25. The momentum distribution has a $\frac{-1}{x^\alpha}$ dependence, the collimator selects a certain distance along the x-axis from this distribution. Therefore for a higher selected momentum a broader range is selected.
Comparing the rates is difficult due to the fact that we have only a small number of events in the experimental area detector. Considering the events after the secondary target we disregard the momentum separation. Anyway we calculate the ratio r of events for different secondary targets behind these targets to those of Cu 10 mm, running the simulation with the same parameters (primary beam with a momentum of 7 GeV, 1250×10000 electrons). The results for the simulation are listed in Table 3.

Material	Hits	Ratio to Cu 10 mm
Cu 10 mm	27725	1
Cu 5 mm	15647	0.56
Al 4 mm	3305	0.12

Table 3: Ratio r of events after the secondary target

The comparison with the experiment can be done by calculating ratios at the same energy between different targets.

Material	Rate at 3 GeV [Hz]	Ratio to Cu 10 mm
Cu 10 mm	8333	1
Cu 5 mm	8105	0.97
Al 4 mm	2567	0.31

Table 4: Ratio r_{1-2} of rates from experiment

As there is a significant difference in the rates, we assume that there are momentum dependent losses between the secondary target and the experimental area. For more precise results further studies taking the data in the experimental area detector into account should be made.
Using the fiber bundle we gain a factor of 1.3 from the simulation, a factor of about 3 in experiment. We assume that the simplification of positioning 5 fibers does not reflect the real situation. It should be mentioned that the exact number of fibers in the experiment bundle is unknown.
Concerning the momentum selecting magnet we give in Figure 28 a rough estimate of the correlation between the magnetic field strength and the outcoming momentum. As

in the experiment there is a linear dependence. It is interesting to see in the beam profile (Figure 26) that the spot of the final beam is not centered along the axis.

7 Conclusion

- We have collected experimental data about the beam characteristics, in particular about the different converter targets, that can be used as a reference for future users of the test beams at DESY.
- We have confirmed the linear dependence of the intensity in the selecting magnet with the momentum of the electrons coming into the experimental hall.
- The detector is well understood and can be used for other electron beam lines at DESY, software for analysing the data is also available. The studies can easily be redone to obtain precise data from the other test beam lines.
- The simulation provides lot of interesting information about the test beam, but it should be runned in a longer basis to have enough statistical data, specially about the rates in the experimental hall detectors for the different targets. Another possibility is to split the simulation apart, using enhanced results of the former part.
- We have confirmed the possibility of using the fiber bundle to obtain higher rates from low current.

Acknowledgement

We would like to thank Ingrid Gregor and Tobias Haas for overseeing our project work. Thanks to Ulli Kötz who helped us with the electronic and hardware part. During the measurements we would like to thank John Maidment for stable beams by shaking his fist at the control room team. Julia Fourletova helped us to repair a broken CPU keeping her busy on her last day at DESY. The authors would like to thank the machine group for their strong support, especially John Maidment.
This work is supported by the Commission of the European Communities under the 6^{th} Framework Programme "Structuring the European Research Area", contract number RII3-026126.

References

[1] Test Beams at DESY *T. Behnke, E. Garutti, I. M. Gregor, T. Haas, U. Kötz, I. A. Melzer-Pellmann, N. Meyners, J. Mnich, F. Sefkow* EUDET-Memo-2007-11

[2] Characterization of the T24 electron beam line available at DESY *D.Auterio, Y. Caffari, L. S. Exposito, A. Marotta, J. Marteau, P. Migliozzi*

[3] Review of Particle Physics *W.-M. Yao et al.* J. Phys. G 33, 1 (2006)

[4] S. Fourletov, Standard Readout Software of MVD Telescope.

[5] Untersuchung der Photonproduktion bei elektron-positron annihilationen am speicherring petra *Karlheinz Meier.* DESY F11-84/01

A Appendix

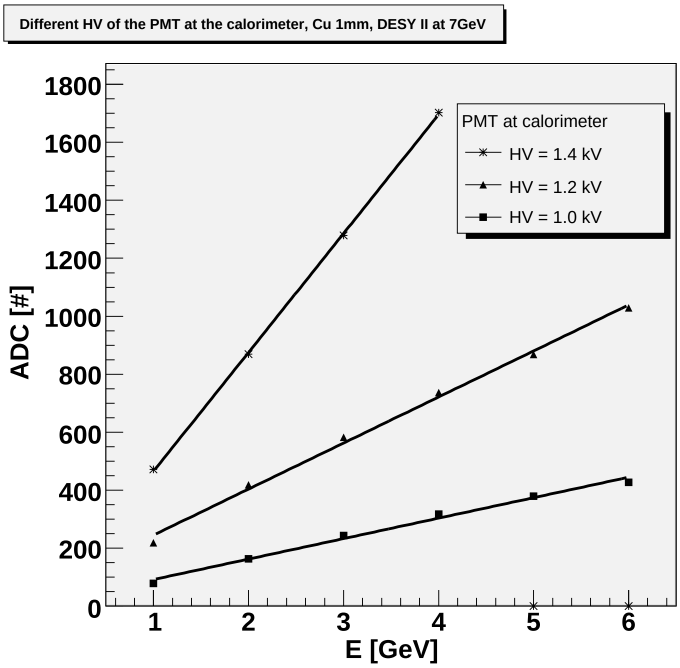

Figure 31: Energy signals at different high voltages for the PMT at the lead glass block.